Full Paper

Wiley Online Library

ELECTROANALYSIS

DOI: 10.1002/elan.202060599

A Molecular Imprinted Polymer Sensor for Biomonitoring of Fenamiphos Pesticide Metabolite Fenamiphos Sulfoxide

Bakhtiyar Qader,[a, b] Issam Hussain,[c] Mark Baron,[b] Rebeca Jimenez-Perez,[b, d] Jose Gonzalez-Rodriguez,*[b] and Guzmán Gil-Ramírez*[b]

Abstract: A new electrochemical method for the identification and quantification of Fenamiphos pesticide's major metabolite in biological samples – Fenamiphos Sulphoxide (**FNX**) was developed. Computational calculations, Density Functional Theory (DFT) and semi-empirical models (PM3) were performed to determine the best monomer, pyrrole, and a ratio of 1:5 (template: monomer) was chosen for the fabrication of the **FNX**–MIP sensor obtained by electropolymerization. The **FNX**–MIP sensor responded well to increasing **FNX** concentrations (range of 1–30 μM). Limit of detection and quantification (LOD = 0.183 μM, LOQ = 0.601 μM), respectively, selectivity, and repeatability were also investigated for the developed method. The obtained percentage of recovery showed good agreement compared to reference values obtained from GC-MS, which was used as a reference method. The **FXN**–MIP sensor proved selective in the presence of potential interferents. The developed sensor was successfully applied for the determination of **FNX** in spiked plasma and urine matrixes with acceptable recovery rates. The proposed method also proved successful in detecting **FNX** prepared from the *in vitro* metabolism of **FNP** using liver microsomes to metabolize it.

Keywords: Fenamiphos · Fenamiphos sulfoxide · pesticide metabolism · MIP · sensors

1 Introduction

Until the 21st century, organophosphorous pesticides were among the most widely used insecticides to protect crops against insects. However, these compounds are an extremely toxic class of chemicals as recognized by the World Health Organization WHO. Organophosphorous (OP) compounds show marked specificity for the acetylcholine esterase enzyme and their interaction inhibits the enzyme activity, preventing hydrolysis of acetyl choline (ACh) [1]. These creates accumulation of ACh causing irreversible harm to the nervous system. Organophosphorous compounds are so effective at harming the nervous system that some potent warfare chemicals (sarin, VX agent) are OP chemicals [2] Due to the extensive use of organophosphate pesticides and their adverse effect on health and environment, it has become very important to develop sensitive, specific, accurate and portable methods of pesticide detection in water and biological fluids. Many traditional analytical chromatographic and spectrometric methods have been exploited for pesticide analysis due to their sensitivity, accuracy and reliability, but they require not only expensive equipment but also highly trained technicians. Therefore, the development of sensors that allow for high sensitivity and selectivity, simple operation, fast response and cheap instrumentation, and can really prove to be an effective alternative to the time-consuming traditional methods is highly desirable. Fenamiphos (*O*-ethyl-*O*(3-methyl-4-methylthiophenyl)-isopropylamido phosphate, **FNP**) is a organophosphorus pesticide that appears as colourless crystal or a tanned waxy solid. **FNP** has local and systemic insecticide activity hence it is widely used to eradicate nematodes and thrips in agricultural soils. **FNP** along with carbendazim are considered pesticides of choice when used in pre-planting, at planting and pre- and post-harvest stages of plant growth [3]. Highly toxic effects have been observed in aquatic and terrestrial organisms, particularly in birds and fish species. Its oxidative metabolites are also categorised as dangerous substances for human health [4]. Fenamiphos undergoes oxidative degradation producing fenamiphos

[a] B. Qader
Sulaimani Medicolegal Institute, Kurdistan Regional Government, Qanat Street, Sulaimani, Iraq
[b] B. Qader, M. Baron, R. Jimenez-Perez, J. Gonzalez-Rodriguez, G. Gil-Ramírez
Joseph Banks Laboratories, School of Chemistry, University of Lincoln, Lincoln LN6 7DL, UK
E-mail: jgonzalezrodriguez@lincoln.ac.uk
ggilramirez@lincoln.ac.uk
[c] I. Hussain
School of Life Sciences, University of Lincoln, Brayford Pool, Lincoln LN6 7TS, UK
[d] R. Jimenez-Perez
Department of Physical Chemistry, Higher Technical School of Industrial Engineering, University of Castilla-La Mancha, Campus Universitario s/n, 02071, Albacete, Spain

Supporting information for this article is available on the WWW under https://doi.org/10.1002/elan.202060599

sulfoxide phenol (**FXP**) and fenamiphos sulfone phenol (**FOP**) (Figure 1) and they are more toxic than the parent compound in both soil and fresh water [5].

A study on the toxic effects of **FNP** in aquatic alga *Pseudokirchneriella subcapitata* and terrestrial alga *Chlorococcum sp.* revealed that **FNP** was metabolised into fenamiphos sulfoxide (**FNX**), fenamiphos sulfone (**FNO**), fenamiphos phenol (**FP**), fenamiphos sulfoxide phenol (**FXP**) and fenamiphos sulfone phenol (**FOP**). Rat liver microsomes have been used for *in vitro* **FNP** metabolism and also identified **FNX** along with other unidentified metabolites [6].

Among all five reported metabolites of **FNP**, **FNX** and **FNO** are regarded as being the major metabolic products [6–7]. They all have similar toxic effects as the parent compound.

Several analytical methods have been used for the determination of **FNP** and its metabolites in a wide range of samples, including nuclear Magnetic Resonance (NMR) [8], high performance liquid chromatography (HPLC) [9], capillary electrophoresis (CE) [10], gas chromatography (GC) [11], and liquid chromatography (LC) [12].

The presence of parent compounds or its main metabolites in biological samples implies the possibility of recent exposure to pesticide toxicity [13]. A HPLC approach was used for the measurement of **FNP** and its metabolites (**FNX** and **FNO**) following *in vitro* metabolic studies using human liver microsomes in a concentrate on range of 1–150 μM [9b]. Furthermore, **FNP** and its two major metabolites were also simultaneously determined by CE in soil samples. A calibration curve for each compound were separately established over a range of 15 to 100 mg/kg, 3 to 30 mg/kg. and 3 to 30 mg/kg with sensitivity of 4.64 mg/kg, 0.55 mg/kg, and 0.89 mg/kg for **FNP**, **FNX**, and **FNO**, respectively [10].

Although chromatographic and non-chromatographic methods are suitable for the analysis, these methods are time consuming, labour-intensive, expensive and require substantially trained staff. To overcome these disadvantages, alternative methods should be inexpensive, simple to operate by low skilled operators, usable in field analysis, and highly sensitive and selective. In addition, the method should be suitable for quantitative analysis and monitoring pesticide residues in the environmental samples as well as provide information about their fate of degradation [4,14].

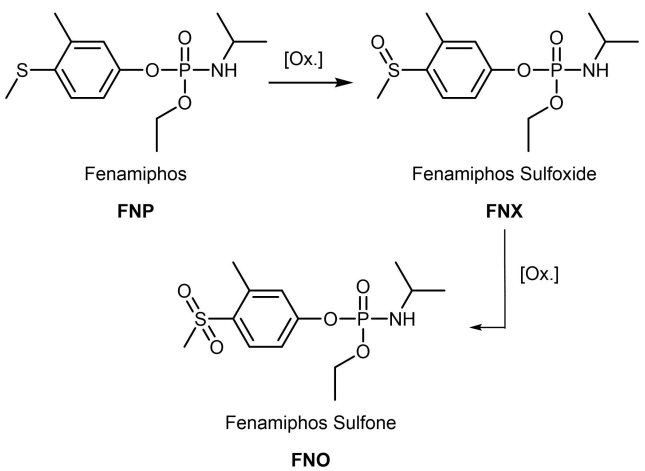

Fig. 1. Breakdown of fenamiphos into its main oxidative metabolites: fenamiphos sulfoxide **FNX** and fenamiphos sulfone **FNO**.

A common and recent strategy to achieve more sensitivity and selectivity for the working electrode consist on its modification using molecularly imprinted polymers (MIP). Furthermore, MIPs are easily prepared, cheap and stable in a wide range of chemical and physical conditions [15]. Herein, a computational approach was applied for the selection of the best interacting monomer with **FNX** and optimization of matching monomer-template ratio was done by semi-empirical calculations at the PM3 level.

To the best of our knowledge only one method has been found in the literature using electrochemical detection for the analysis of fenamiphos sulfoxide [16]. Although the method can be used for the analysis of biological samples, the proposed method herein using MIPs has demonstrated greater robustness to interferences and higher selectivity presenting also a lower limit of detection. The method developed here opens the possibility of cheap, fast determination of this pesticide's metabolite in biological samples. The portability and simplicity can make it suitable for field application in the areas of health and/or environmental monitoring and even chemical warfare detection as organophosphorus compounds have been used as chemical warfare agents [2].

2 Materials and Methods

Hydrochloric acid, phosphoric acid, glacial acetic acid and potassium hydroxide, acetonitrile (HPLC grade), sodium perchlorate, lithium perchlorate, G6PDH, potassium monophosphate and potassium phosphate dibasic were purchased from Fisher Scientific (Fisher Scientific, UK); Potassium ferric cyanide, artificial human plasma, sodium chloride, Fenamiphos, fenamiphos–sulfoxide, fenamiphos–Sulfone, 2-isopropoxyphenol, strychnine, disulfoton–sulfoxide, pyrrole and magnesium chloride were bought from Sigma (Sigma Aldrich, UK). Britton-Robinson buffer (BRB) solution comprised phosphoric acid, glacial acetic acid and sodium chloride; the pH value was adjusted with sodium hydroxide and hydrochloric acid. Silica (particle size 0.007 μm) and aluminium oxide (particle size 0.05 μm) used for polishing the glassy carbon electrode, were both bought from Sigma-Aldrich (Sigma-Aldrich, UK). Deionized water was obtained using an ELGA purification system to a specific resistance 18 MΩ/cm and used to prepare all solutions. Urine aliquot was provided by a volunteer. Pig liver was obtained freshly from a local abattoir, kept in ice cold and transferred directly to the laboratory for processing minimizing the

time for preparation. The NADPH regeneration system, nicotinamide adenine dinucleotide phosphate (NADP and glucose-6-phosphate (G6P), were purchased from Sigma (UK). Glucose-6-phosphate dehydrogenase enzyme (G6PD) was obtained from Bio-Rad. Biuret reagent, composed of allophanamide solution treated with sodium hydroxide and cupric sulphate, was prepared in house.

2.1 Electrochemistry and Gas Chromatography

Differential pulse voltammetry (DPV) measurements were performed on a modified GC electrode using the following parameters: potential range, 0.6 to 1.3 V; voltage step, 10 mV; pulse amplitude, 50 mV; pulse time, 0.04 s; voltage step time, 0.4 s; and sweep rate, 0.0248 V/s. The glassy carbon electrode was polished to a mirror-like surface by grinding successively with aluminum oxide and silica slurry prior to running all experiments.

GC-MS analyses were performed under the following programme: oven temperature started at 100 °C held for 1 min. then increased at 25 °C/min to 200 °C then held for 2 min., then a ramp of 10 °C/min was used to reach a final temperature of 310 °C and held for 2 mins using helium as the carrier gas at 1 mL/min. Injection volume was 2 µL. The transfer line temperature was held at 300 °C. Ionization was achieved by electron impact (EI+) source at 200 °C with electron energy of 70 eV and the multiplier was set to 350 V under positive ionization mode. The peaks were observed in total ion count (TIC) mode after 2 minutes' solvent delay giving a total run time of 20 minutes.

2.1.1 Instruments and Apparatus

Voltammetric experiments were performed using a Metrohm 757 VA Computrace (Metrohm Ltd., UK), using software version 1.0 Ct757 for data processing (Metrohm Ltd., UK). A conventional three electrode system was used for all the experiments, which consisted of a glassy carbon (GC) electrode as the working electrode, a Ag/AgCl electrode serving as reference electrode, and platinum as an auxiliary electrode, all electrodes were purchased from Metrohm (Metrohm Ltd., UK). Buffer solutions were prepared using a digital pH meter (Hanna precision pH meter Model pH 210). Electrode sonication was carried on an ultrasound bath (Kerry, UK).

GC-MS were performed on a Perkin Elmer Clarus 500 instrument equipped with an auto sampler and operated with software TurboMass (2008). Analytical samples and Standards were run on an SUPELCO analytical, SLB-5m fused silica capillary column (30 m × 0.25 mm × 0.25 µm).

2.1.2 Preparation of Solutions

A 30 mM standard stock solution of FNX was prepared by adding 250 mg of it into 27.5 mL in acetonitrile. A 15 mM standard stock solution of FNP was prepared by adding 100 mg of the substance into 20.9 mL in acetonitrile. Standard stock solutions were stored at −8 °C in amber bottles. All other working solutions were freshly prepared from the standard stock solution. The prepared concentrations to prepare the calibration regression were labelled and stored in white plastic bottles and stored in amber bottles in the fridge until required. Britton-Robinson buffer (BRB) is an aqueous universal buffer that was used for the pH study in the range of 1.6 to 12. One litre of 0.5 M of BRB was prepared adding 33.8 mL of concentrated phosphoric acid (14.8 M), 28.6 mL of concentrated acetic acid (17.48 M) and 29.22 grams of sodium chloride into one litre of distilled water. The pH value was adjusted with sodium hydroxide and hydrochloric acid. The rest of buffers and supporting electrolytes were freshly prepared in distilled water just before usage.

The extraction solution for removal of the template was made of 2 volumes of acetic acid and 5 volumes acetonitrile. The polymerisation solution was prepared by mixing 10 mM pyrrole and 2 mM **FNX** in 100 mM BR buffer solution.

2.1.3 Electropolymerization Procedures

Prior to the electro-polymerization, the GC electrode was polished to a mirror-like surface successively with aluminum oxide and silica slurry and then sonicate in methanol for 2 minutes. An electrolyte solution that contained 10 mM pyrrole, 2 mM **FNX**, and 100 mM BR buffer solution was used for the electro polymerization by cyclic voltammetry in a potential range of 0 V to +1.2 V (vs Ag/AgCl) with a scan rate of 0.05 Vs^{-1} for 7 scan cycles, after initial purging of the mixture under nitrogen gas for 300 seconds. The **FNX** molecules were removed from the polymeric film by immersing the MIP electrode into a stirred mixture of acetic acid and acetonitrile at a ratio of 2:5 (v/v). Finally, the molecularly imprinted GC electrode was then dried by blowing under nitrogen gas. The non-imprinted polymer (NIP) was prepared by following the same electro-polymerization and template removal steps but without the presence of the template molecule, **FNX**, in the electrolyte mixture of the electro-polymerization step.

3 Results and Discussion

3.1 Computational Calculations for the Selection of MIP Monomers

To obtain a good, selective MIP the formation of a complex between the targeted guest and a suitable functional monomer is key. Computational methods were selected as a manner to screen the affinity of potential monomers (Figure 2) instead of an experimental evaluation of complexation energy. Computational methodologies suffer from hard drawbacks and provide only a rough estimation of the affinity due to caveats not easily

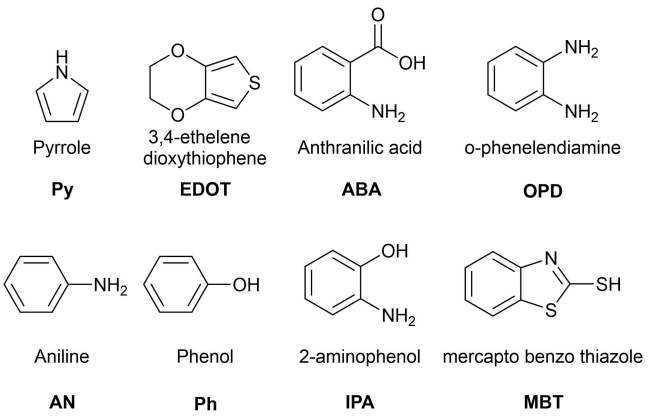

Fig. 2. Chemical structures of the monomers used for the computational calculations.

addressable in a model system that uses only one monomer molecule. Computational methods consider an interaction at vacuum, while solvation/desolvation effects will play a role in the experimental evaluation of the affinity. High level calculations that consider solvent effects or more than one monomer molecule, or complex models to fit the data that account for the binding energy of more than one monomer to the analyte are possible, but they were beyond the scope of this work. The computational approach was selected due to being faster and cheaper. Monomer selection was explored at the density functional theory (DFT) level using B3LYP functional in combination with the 6-31G basis set. The conformational optimization of the **FNX** template molecule and eight functional monomers (Figure 2) [(phenol (**Ph**), pyrrole (**Py**), aniline (**AN**), 2-aminophenol (**IPA**), anthranilic acid (**ABA**), 3,4 ethelenedioxythiophen (**EDOT**), *o*-phenelendiamine (**OPD**), mercaptobenzothiazole (**MBT**)] that can be electrochemically polymerised on a glassy carbon electrode were studied.

One molecule of each monomer was separately paired with one **FNX** molecule in vacuum [17], and the binding energy of the template-monomer complex, ΔE, was calculated based on equation 1 [18]:

$$\Delta E = E(\text{template-monomer}) - E(\text{template}) - \sum E(\text{monomer}) \quad (1)$$

Computational calculations showed that all monomer-template pairs presented a favourable negative energy, as expected at vacuum. The **FNX**–**Py** pair displayed the highest absolute ΔE value indicating **Py** had a strong interaction with **FNX** template while the **Ph**–**FNX** interaction was the weakest. Therefore, **Py** was selected as the monomer for designing a **FNX** selective MIP. Nevertheless, the comparison was not aimed at obtaining an accurate picture of the binding energies but an approximate comparative value among the template and the different monomers to select a suitable combination.

3.2 Fabrication of the FNX Imprinted Sensor

The MIP film was prepared by electro polymerisation on the surface of bare GC electrode using CV in a potential range −0.6 to 1.0 V and scan rate 100 mV/S in Britton-Robinson (BR) buffer solution (pH, 6) [19]. Figure 3 shows a typical cyclic voltammogram recorded during the synthesis of MIP and NIP films. During the electropolymerization of **Py** in the absence of the template, the oxidation of **Py** started at 0.85 V potential in the first cycle and the oxidation peak intensity increased progressively on subsequent cycles, indicating polymeric film growth on the working electrode [20]. Compared with NIP, the oxidation of **Py** in the presence of **FNX** was delayed at first cycle with a lesser peak current intensity and in consecutive cycles did not progressively increase due to trapped **FNX** molecules into the polymer.

Furthermore, the intensity of the anodic peak of **Py** increased at the first cycle and did not progressively decrease in the following cycles due to the trapping of **FNX** molecules into the polymer.

The NIP and the **FNX**–MIP showed different electrochemical profiles (Figure 3). It was expected that reversible interactions were established between the imprinted polymer film and **FNX**. Indeed, these reversible interactions were demonstrated later (Figure 4) when the template was easily removed and reloaded before analysis by DPV. The oxygen and/or sulfur in the **FNX** molecules could interact with the hydrogens of the pyrrole NH group in the polymer by hydrogen bonds and/or other possible non-covalent inter-molecular interactions.

3.3 FNX–MIP Sensor Voltammetry

The MIP developed sensor and the non-imprinted polymer (NIP) were both investigated by DPV under the same conditions as shown in Figure 3. The signal intensity of the peak in the MIP sensor was larger than the bare

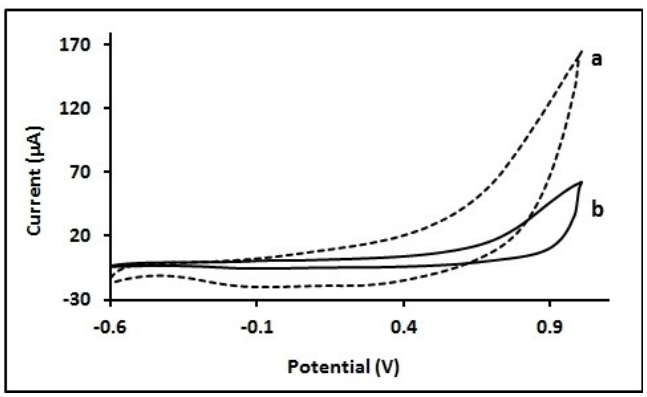

Fig. 3. Cyclic voltammograms obtained during the preparation of a) Non-imprinted polymer; b) **FNX**-imprinted polypyrrole films at GC electrode. Experimental conditions: [**Py**] = 10 mM; [**FNX**] = 2 mM; scan rate = 50 mV/s; [BR buffer] = 0.1 M; number of cyclic scans = 7.

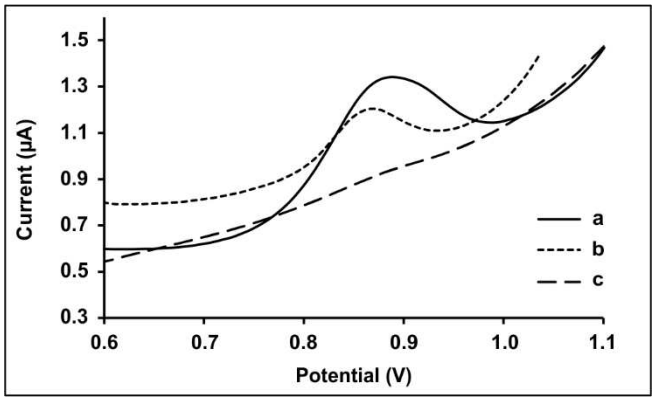

Fig. 4. Differential pulse voltammetry of 10 μM **FNX** in 0.1 M BR buffer solution a) on **FNX**–MIP sensor; b) on bare GC electrode and c) FNX on NIP supported on GC electrode.

GC electrode, 1.8 and 0.8 μA respectively after baseline correction, using the same 10 μM concentration, suggesting that the MIP sensor is more sensitive than the bare electrode. In contrast, the signal intensity for the NIP was much lower, 0.0091 μA, than the bare GC electrode most likely due to less efficient electron diffusion to the electrode. The voltammetric response of the MIP sensor was also studied in BR buffer (pH = 6) solution; the peak current increased with increasing concentration of **FNX** in the solution when analyzed by DPV as seen in Figure 4. The peak currents were proportional to the concentration of **FNX** in the range of 1–30 μM (See S.I.).

The LOD was calculated using 3*S*/P and the LOQ was calculated as 10*S*/P, where *S* is the standard deviation of nine measurements of the lowest concentration of **FNX** and P is the slope of the linear regression. The observed LOD and LOQ for **FNX**–MIP were 0.183 μM and 0.601 μM, respectively, suggesting that the LOD of the developed sensor is lower than the bare GC electrode.

Hence, the developed **FNX**–MIP electrode for the determination of **FNX** presented enough sensitivity to be applied for the biomonitoring of **FNP** exposure through its metabolites [13a,21]. Furthermore, the sensitivity of the proposed electrochemical method is better than HPCL (1.0 μM) [9b] and Capillary Electrophoresis (1.6 μM) [10] which have been reported for the analysis of **FNX** in *in vitro* and soil samples respectively.

The precision of **FNX**–MIP fabricated sensor was assessed by calculating the percentage relative standard deviation (% RDS) for 5 repeated measurements on the same day (intra-day precision) and 5 consecutive days (inter-day precision). The precision was calculated using different concentrations (1–30 μM) of **FNX** by DPV as shown in Table 1. In general, the precision results were in the 1.47–13.46 % and 3.57–14.39 % range for intra-day and inter-day measurements, respectively. In both cases, intra- and inter-day, the less precise results correspond to the 1 μM concentration. When considering the 5–30 μM range the precision increases noticeably and is under 3.52 % and 7.57 % for the intra- and inter-day, respectively. The small spread of % RSD, under 14.39 %, within the concentration range studied, suggested that the developed sensor is precise.

Table 1. Intra-day and inter-day precision in the 1–30 μM concentration range of **FNX**. DPV measurements using the **FNX**–MIP sensor.

Concentration (μM)	Intra-day precision Mean ± SD (μM)	RSD (%)	Inter-day precision Mean ± SD (μM)	RDS (%)
1	1.8 ± 1.1	13.46	1.4 ± 1.1	14.39
5	5.9 ± 0.5	3.24	6.5 ± 1.1	6.31
10	10.9 ± 0.8	3.52	10.6 ± 1.8	7.57
15	16.1 ± 0.6	1.92	14.7 ± 1.5	4.90
20	22.8 ± 0.7	1.48	20.4 ± 2.1	5.22
25	25.5 ± 0.5	1.58	23.7 ± 1.6	3.57
30	28.9 ± 0.8	1.47	28.0 ± 2.2	4.04

The repeatability of the imprinted electrode was compared with that of the bare glassy carbon electrode for a concentration of 20 μM. In general, the results depicted that the precision of the MIP sensor is better than the precision of the non-modified electrode. Also, the MIP sensor exhibited high reproducibility and was very stable for at least 5 days with subsequent cycles of washing and measuring operations.

The sensor recovery rate was evaluated using the same concentration range (1–30 μM) of **FNX** by DPV as shown in Table 2. The recovered concentration was calculated from the calibration curve for the mean of three repeated measurements. The recovery rate observed within the concentration range is larger than 97.96 %, indicating that the developed sensor is reliable for real applications.

To validate the developed method, the same **FNX** solutions measured with the **FNX**–MIP electrode were also measured by GC-MS and this method was used as a reference method to compare recovery results from the proposed electrochemical method as seen in Figure 5. The relationship between the two methods was linear with a slope close to 1 and an intercept close to zero, indicating that the two methods were statistically similar ($y = 1.02 + 0.07$; $r^2 = 0.988$).

The selectivity of the **FNX**–MIP sensor toward the anodic peak of **FNX** in the presence of four potential

Table 2. Recovery rate for concentration range (1–30 μM) of **FNX** measured using DVP on the **FNX**–MIP electrode.

Concentration (μM)	Mean ± SD (μM)	RSD (%)	Recovered (%)[a]
1	1.0 ± 0.1	12.76	104.1
5	5.4 ± 0.5	8.93	107.5
10	9.9 ± 0.1	1.34	98.9
15	15.0 ± 0.1	1.01	99.9
20	19.6 ± 0.4	2.03	98.0
25	24.6 ± 0.3	1.08	98.3
30	30.1 ± 0.9	2.89	102.1

[a] Recovered concentration is the average of three repetitions.

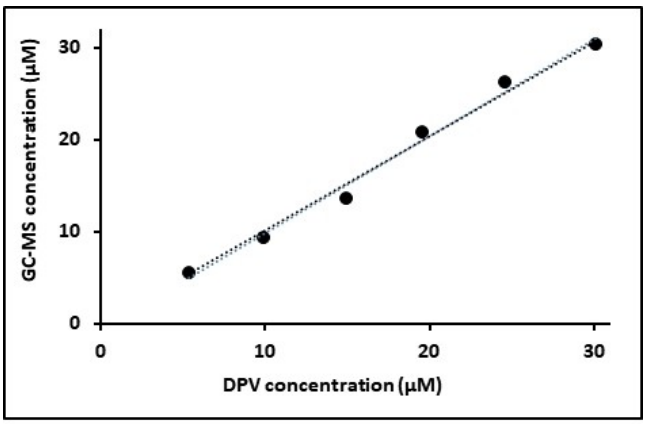

Fig. 5. Statistical correlation between reference method (GC-MS) for **FNX** and the developed **FNX**–MIP electrochemical method using DPV.

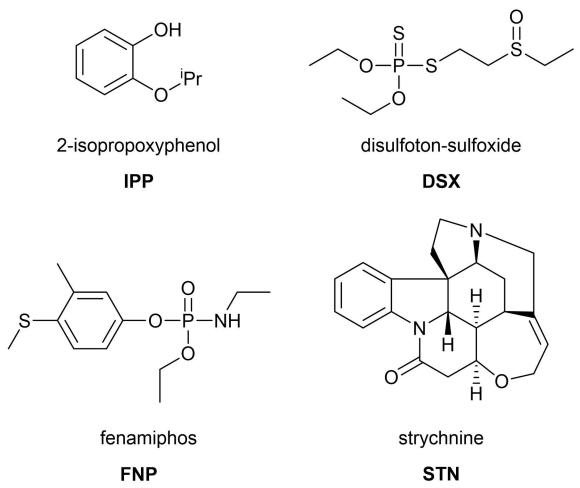

Fig. 6. Molecular structures for the interferents considered.

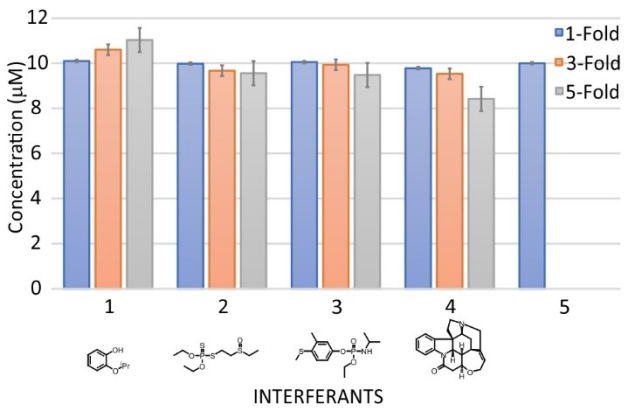

Fig. 7. Concentration recovered from a 10 µM **FNX** solution with the **FNX**–MIP sensor calculated from the current changes in presence of 10 µM (one-fold), 30 µM (three-folds) and 50 µM (five-folds)) of the selected interferents: (1) 2-isopropoxyphenol, (2) Fenamiphos, (3) Strychnine, (4) Disulfoton–sulfoxide, and (5) Fenamiphos–sulfoxide with no interferences.

interferences in the electrochemical determination of **FNX** was also studied. Interferent compounds (Figure 6): 2-isopropoxyphenol (**IPP**), disulfoton–sulfoxide(**DSX**), fenamiphos (**FNP**), and strychnine (**STN**) were selected because these substances have oxidation peaks close to that of **FNX** or being structurally similar to **FNX** particularly **DSX** and **FNP**. The influence of each separate substrate on the oxidation peak of **FNX** using the **FNX**–MIP sensor was investigated using DPV. The current response for the **FNX** oxidation peak in the presence of the interferents at three different concentrations (10, 30 and 50 µM) were recorded. The comparison in the current response of a 10 µM solution of **FNX** in the presence and absence of each interfering substances by DPV is shown in Figure 7. None of the spiked interfering elements showed a significant interference in the **FNX** detection. The worst result showed a 15.8 % decrease in signal when **FNX** was determined under a 5-fold excess of **DSX**. Only one of the interferents, **IPP**, showed that with increasing concentrations of the interfering species the current response increased, indicating that more than 5-fold of **IPP** could influence sensor selectivity. These results confirm that the sensor has a high selectivity even in presence of up to five folds' interference species due to the highly specific recognition between the MIP binding sites and the **FNX** molecules.

3.4 Application of the FNX–MIP Sensor in a Biological Matrix

To evaluate the validity of the proposed electrochemical method for the determination of **FNP** major metabolite (**FNX**) in real samples, human plasma and urine samples were spiked with known amounts of **FNP** or **FNX**. Plasma and urine sample solutions were prepared using BR buffer (see SI) and **FNP** or **FNX** were added into the plasma and urine sample solutions before measuring with CV or DPV using the bare GC electrode or the developed **FNX**–MIP sensor. A calibration plot for each of the methods was used to calculate the recovered concentration of the spiked samples. Table 3 includes the results obtained from DPV analysis with the **FNX**–MIP sensor for the different spiked concentrations of **FNX** in urine and plasma samples. The recovery rate in both matrixes (urine, plasma) was similar and in the range of 88.62–95.23 % with the % RSD value being less than 11.75 %.

Table 3. Average **FNX** recovery on urine and plasma samples spiked with a known concentration of **FNX** measured by DPV with the **FNX**–MIP sensor. Samples were prepared using two different concentrations: 15 and 25 µM.

	Plasma		Urine	
Spiked (µM)	15	25	15	25
Recovered (µM)	13.29	23.71	13.49	23.80
Recovered (%)	88.62	94.84	89.94	95.23
RSD (%)	11.75	2.36	2.75	1.76

The samples with higher concentration displayed better recovery (>94 %) than the lower concentration samples. As a matrix, plasma had a slightly worse effect indicated by around 1 % lower recovered concentration and a much larger RSD (11.75 %) for the lower concentration sample. Thus, the results showed that the matrix did not significantly influence the recovered concentration and urine matrix had a slightly less detrimental effect on recovered concentration than plasma.

In order to further test the viability of the developed MIP electrochemical method on biological samples, the **FNX**–MIP sensor was used for the determination of **FNX** in samples that were prepared using an *in vitro* metabolic pathway of the **FNP** metabolism using pig microsomes. Incubated samples from the *in vitro* metabolism of **FNP** using pig liver microsomes were prepared and reconstituted with BR buffer (pH 6) solution. The samples were measured in triplicate by DPV where the initial **FNP** concentration was measured using a previously developed GC electrode method [16] and the **FNX** produced as a result of the metabolic process was detected using the **FNX**–MIP sensor. Samples with two different initial concentrations of **FNP** were prepared and measured ($N=3$): sample A – **FNP** 50 μM and B – **FNP** 100 μM. The **FNX**–MIP sensor was able to selectively detect the production of **FNX** from an initial concentration of **FNP**. The detected concentrations were low for both samples: sample A – 8.82 μM, 7.94 % RSD; sample B – 12.79 μM 5.02 % RSD. This could be explained by the fact that the metabolic pathway might give rise to other possible metabolites from **FNP**, as discussed before, other oxidation or hydrolysis products are possible which are not detected by the **FNX**–MIP sensor. Nevertheless, the sensor proved capable of detecting the metabolite **FNX** obtained from the metabolic reaction, indicating that can be used to detect selectively **FNX** metabolite in urine or plasma samples.

4 Conclusion

A molecularly imprinted sensor was designed for fenamiphos sulfoxide using Density Functional Theory (DFT) and semi-empirical models (PM3) calculations. The best matching monomer was found to be pyrrole, and a ratio, 1:5 (template: monomer) was chosen for the fabrication of **FNX**–MIP sensor. The working electrode was modified by electro polymerization of the optimized monomer-template mixture using CV. The developed sensor showed improved analytical response towards **FNX** compared to that of the glassy carbon electrode. Sensitivity, selectivity, and repeatability were also investigated for the developed methods in biological samples showing a good response. The obtained percentage of recovery showed good agreement compared to those reference values when GC-MS was used as a reference method. The developed sensor was successfully applied for the determination of **FNX** in spiked plasma and urine biological samples with acceptable recovery rates. The selectivity of the developed **FNX**–MIP sensor was evaluated in the presence of potential interferents, showing high selectivity toward **FNX** molecules even in presence of structurally related interferants. The proposed method was also applied to the determination of **FNX** from samples prepared from the *in vitro* metabolism of fenamiphos using pig liver microsomes in the presence of NADPH as a regenerating system. The results were monitored using the developed electrochemical system, showing that the work developed here opens the door to the production of easy-to implement analytical systems for the analysis of fenamiphos metabolites on biological samples such as urine or plasma.

Acknowledgements

The authors gratefully acknowledge the financial support to this work by the Higher Committee for Educational Development (HCED number D-11-3277), Iraq.

Data Availability Statement

The data that support the findings of this study are available from the corresponding author upon request.

References

[1] T. Namba, *Bull. W. H. O.* **1971**, *44*, 289–307.
[2] in *The Chemistry of Organophosphorus Chemical Warfare Agents*, **1996**, pp. 781–840.
[3] G. N. Agrios in *chapter nine – CONTROL OF PLANT DISEASES*, (Ed. G. N. Agrios), Academic Press, San Diego, **2005**, pp. 293–353.
[4] T. Lima, H. T. D. Silva, G. Labuto, F. R. Simões, L. Codognoto, *Electroanalysis* **2016**, *28*, 817–822.
[5] C. C. Truman, R. A. Leonard, A. W. Johnson, *Trans. ASAE* **1998**, *41*, 663–671.
[6] T. P. Cáceres, M. Megharaj, R. Naidu, *Ecotoxicology* **2011**, *20*, 20–28.
[7] T. Cáceres, M. Megharaj, R. Naidu, *Sci. Total Environ.* **2008**, *398*, 53–59.
[8] F. Molaabasi, Z. Talebpour, *J. Agric. Food Chem.* **2011**, *59*, 803–808.
[9] a) A.-L. Damianys, M.-S. M. Fernanda, O.-H. M. Laura, V.-D. Rafael, M.-N. Antonio, *Toxicol. in Vitro* **2013**, *27*, 681–685; b) N. C. P. de Albuquerque, J. V. de Matos, A. R. M. de Oliveira, *J. Chromatogr.* **2016**, *1467*, 326–334.
[10] M. Lecoeur-Lorin, R. Delépée, P. Morin, *Electrophoresis* **2009**, *30*, 2931–2939.
[11] a) J. Hernández-Borges, J. C. Cabrera, M. Á. Rodríguez-Delgado, E. M. Hernández-Suárez, V. G. Saúco, *Food Chem.* **2009**, *113*, 313–319; b) H. Dahshan, A. M. Megahed, A. M. M. Abd-Elall, M. A.-G. Abd-El-Kader, E. Nabawy, M. H. Elbana, *J. Environ. Health Sci. Eng.* **2016**, *14*, 15.
[12] M. Asensio-Ramos, G. D'Orazio, J. Hernandez-Borges, A. Rocco, S. Fanali, *Anal. Bioanal. Chem.* **2011**, *400*, 1113–1123.
[13] a) J. Hardt, J. Angerer, *J. Anal. Toxicol.* **2000**, *24*, 678–684; b) L. Schmidt, J. Müller, T. Göen, *Anal. Bioanal. Chem.* **2013**, *405*, 2019–2029; c) M. S. Forde, L. Robertson, E. A. Laouan Sidi, S. Côté, E. Gaudreau, O. Drescher, P. Ayotte, *Environ. Sci. Process Impacts* **2015**, *17*, 1661–1671.

[14] a) Y. Ni, P. Qiu, S. Kokot, *Anal. Chim. Acta* **2005**, *537*, 321–330; b) R. F. França, H. P. M. de Oliveira, V. A. Pedrosa, L. Codognoto, *Diamond Relat. Mater.* **2012**, *27–28*, 54–59.
[15] a) S. A. Piletsky, A. P. F. Turner, *Electroanalysis* **2002**, *14*, 317–323; b) M. C. Blanco-López, M. J. Lobo-Castañón, A. J. Miranda-Ordieres, P. Tuñón-Blanco, *TrAC Trends Anal. Chem.* **2004**, *23*, 36–48; c) Z. Zhao, Y. Teng, G. Xu, T. Zhang, X. Kan, *Anal. Lett.* **2013**, *46*, 2180–2188.
[16] B. Qader, M. G. Baron, I. Hussain, R. P. Johnson, J. Gonzalez-Rodriguez, *Monatsh. Chem.* **2019**, *150*, 411–417.
[17] S. K. Mamo, M. Elie, M. G. Baron, J. Gonzalez-Rodriguez, *ACS Appl. Polym. Mater.* **2020**, *2*, 3135–3147.
[18] A. Nezhadali, M. Mojarrab, *Sens. Actuators B: Chem.* **2014**, *190*, 829–837.
[19] J. Gonzalez-Rodriguez, S. K. Mamo, *Sensors* **2014**, *14*, 23269–23282.
[20] N. Belhadj Tahar, A. Savall, *J. Appl. Electrochem.* **2011**, *41*, 983–989.
[21] T. Berman, T. Göen, L. Novack, L. Beacher, L. Grinshpan, D. Segev, K. Tordjman, *Environ. Int.* **2016**, *96*, 34–40.

Received: February 25, 2021
Accepted: February 28, 2021
Published online on ■■, ■■

FULL PAPER

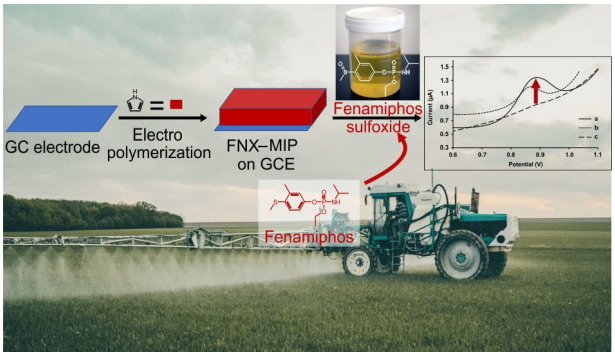

B. Qader, I. Hussain, M. Baron, R. Jimenez-Perez, J. Gonzalez-Rodriguez, G. Gil-Ramírez**